ERCA - Volume 4 - pages 237 to 256
From Weather Forecasting to Exploring the Solar System
Edited by C. Boutron

CHAPTER XIII

Aeronomical Effects of Solar Radiation

G. Kockarts

Institut d'Aéronomie Spatiale, 3 avenue Circulaire, 1180 Bruxelles, Belgique

Abstract. This tutorial paper describes the effects of solar radiation on the terrestrial atmosphere. However, the concepts presented here are valid for any planetary atmosphere. An analysis of the electromagnetic energy output of the Sun is presented in relation with geometric effects and solar activity. The primary actions of solar radiation are described as well as how the radiation is absorbed by atmospheric constituents. Since some absorption cross sections vary strongly with wavelength and temperature, a special treatment must be given to the constituents having such characteristics.

1. INTRODUCTION

Aeronomy is the science dealing with the atmospheric regions where photodissociation and photoionization processes play a role. The word aeronomy, invented by Sidney Chapman, was officially introduced during the general assembly of the International Union of Geodesy and Geophysics held in Roma in 1954. At that time the International Association of Magnetism and Electricity changed its name into International Association of Geomagnetism and Aeronomy. However, aeronomical studies were already going on many years before the official recognition of this discipline.

As an example, the presence of helium at ground level was known since 1895. Knowing this experimental fact, Chapman and Milne (1920) investigated its possible effect on the atmospheric composition at great heights and they assumed that diffusive separation starts at 20 km altitude. Although we know that this assumption is incorrect, the idea to introduce diffusion separation at some altitude is correct. The interested reader who has no access to Chapman

and Milne's original paper can find a redrawing of their results in Kockarts (1973).

Photodissociation and photoionization imply the existence of an energy source of electromagnetic waves. The Sun is the best candidate in our planetary system. Although particle precipitation, like in the auroral regions (see Lilensten, 1996), can also dissociate and ionize atmospheric constituents, we consider here only the effects of solar radiation. Therefore, the characteristics of this radiation is described in section 2. The total energy available at the top of the atmosphere is discussed in sections 3 and 4. Since the energy output is not constant with time, section 5 gives an introduction to variability of the Sun. The basic effects of the solar radiation on atmospheric constituents are presented in section 6, whereas section 7 shows how the radiation penetrates into the atmosphere. Finally, section 8 introduces the problems encountered when the absorption cross sections are characterized by a strong structure and eventually by a temperature dependence. The interested reader in a broad overview of the major aeronomical problems may consult two recent books (Lilensten and Blelly, 1999, Kockarts, 2000).

2. BLACK BODY, RADIANCE AND IRRADIANCE

Although we know that the Sun emits ionized particles which form the solar wind (see Lilensten, 1999), we consider only electromagnetic radiation and its primary effects on the atmosphere. The most simple approach is to consider the Sun as a perfect *black body*. This means that the Sun would be a perfect absorber and a perfect emitter for all electromagnetic waves. At the end of the 19th century, scientist were confused by the available theory which predicted an infinite quantity of energy emitted when wavelength tends towards zero. This is of course in contradiction with observation.

Planck (1901) discovered the correct expression for the *radiance* L_λ which is defined as the energy emitted by a black body at absolute temperature T per time unit, per surface unit, per solid angle unit and per wavelength unit. Planck's law can be written as

$$L_\lambda = \frac{C_1}{\lambda^5 \times \{\exp[C_2/(\lambda \times T)] - 1\}} \tag{1}$$

where λ is the wavelength of the electromagnetic radiation and T is the temperature of the black body.

The constants C_1 and C_2 in equation (1) depend on the units you are using. If L_λ is given in W m^{-2} sr^{-1} μm^{-1} the constant C_1 is 1.1913×10^8 W m^{-2} sr^{-1} m^{-4} and the constant C_2 is 1.4388×10^4 μm K. In this case the wavelength λ must be given in μm.

Although Planck's formula is correct, Bose (1924) pointed out that the derivation is inconsistent with quantum theory, since photons do not obey Boltzmann statistics but obey to what will be called later Bose statistics.

Figure 1 shows the radiance obtained for different black body temperatures.

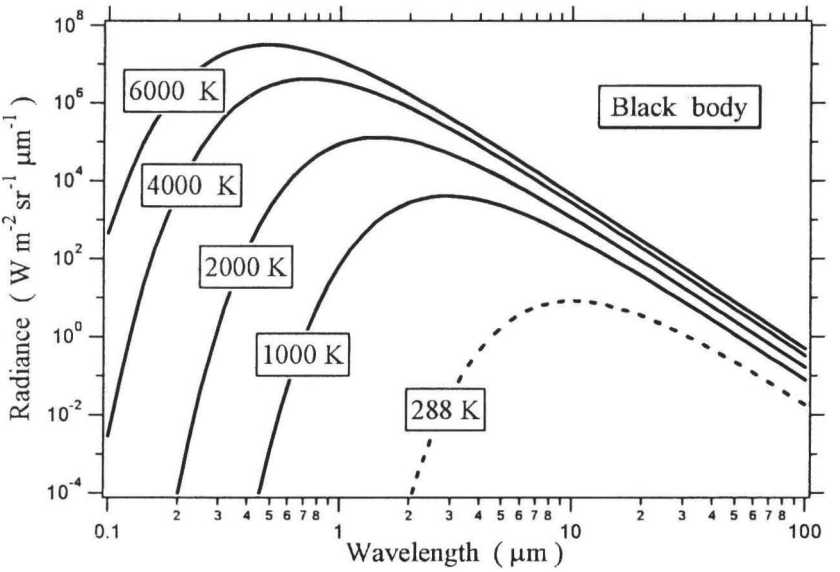

Figure 1. Radiance for different blackbody temperatures.

The visible spectrum extends approximately from 0.4 μm to 0.7 μm and this wavelength domain should correspond to the blackbody temperature of the Sun, i.e. a value between 4000 K and 6000 K (full curves on the figure). The dashed curve corresponds to the average surface temperature (288 K) of the Earth. The maximum is now in the infrared. The fact that the maximum of the solar radiance is at a much shorter wavelength than the maximum of the Earth's radiance allows us to treat these two emissions independently.

Since the Sun–Earth distance is approximately 1.5×10^6 km, we must know how much energy is available at the top of our atmosphere. Another quantity is used for that purpose. It is the *irradiance* which gives the amount of energy received by a unit surface, per unit time and per unit wavelength. The irradiance is, therefore, measured in W m^{-2} μm^{-1}. Viewed from the Earth, one sees the Sun in a solid angle Ω given by

$$\Omega = \pi \times r_s^2/R^2 \tag{2}$$

where $r_s = 6.9598 \times 10^5$ km is the apparent radius of the Sun and R is the time dependent Sun–Earth distance. The mean Sun–Earth distance is called the *astronomical unit* (1 AU $= 1.496 \times 10^8$ km).

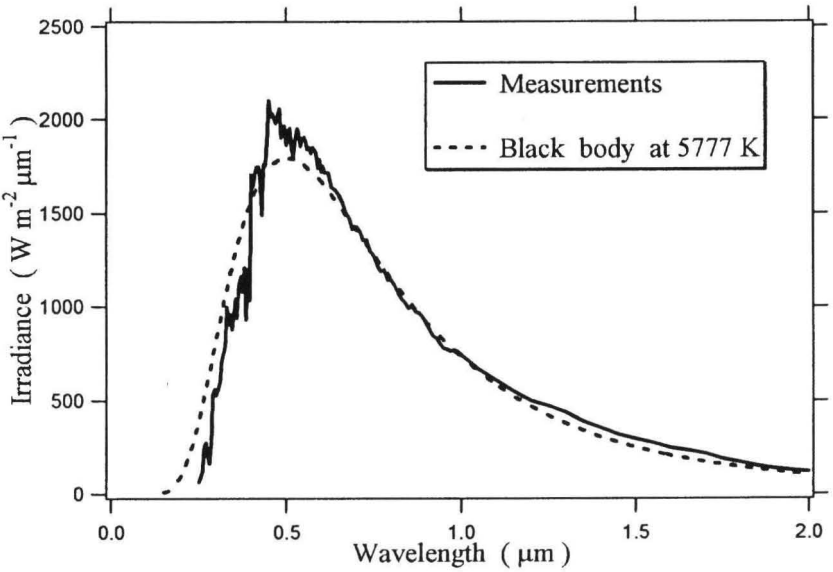

Figure 2. Irradiance measured at the top of the atmosphere compared with theoretical values for a solar blackbody temperature of 5777 K.

The irradiance E_λ can now be expressed as a function of the radiance L_λ by the relation

$$E_\lambda = L_\lambda \times \Omega \tag{3}$$

The full curve on Figure 2 shows the spectral irradiance measured at the top of the atmosphere (Iqbal, 1983) when no radiation is absorbed by atmospheric constituents. The dashed curve is obtained from equation (3) with a solar black body temperature of 5777 K. The two curves have a similar aspect although significant differences can be seen.

3. SOLAR CONSTANT AND ORBITAL ECCENTRICITY

When the measurements of Figure 2 are numerically integrated from 0 to 25 μm, one finds an irradiance $E_s = 1367$ W m^{-2}. The *solar constant* is defined as the total energy received at 1 AU per unit time on a unit surface perpendicular to incident radiation. Equation (3) can be analytically integrated over λ from 0 to ∞. In such a way, a theoretical expression of the solar constant E_s is given by

$$E_s = \frac{r_s^2}{R^2} \times \left(\frac{\pi^5 C_1}{15 C_2^4}\right) \times T^4 = \frac{r_s^2}{R^2} \times \sigma \times T^4 \tag{4}$$

where σ is *Stefan–Boltzmann's* whose value is 5.67×10^{-8} W m^{-2} K^{-4}.

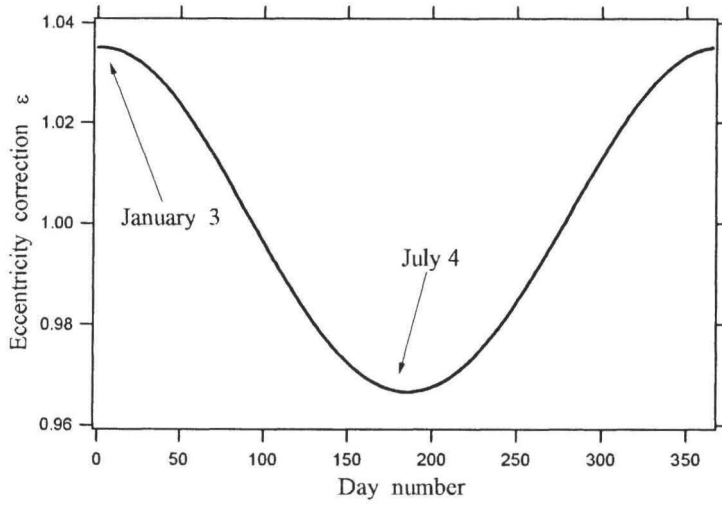

Figure 3. Eccentricity correction for irradiance at 1 AU.

If the measured value $E_s = 1367$ W m^{-2} is introduced in equation (4), one obtains the black body temperature of 5777 K used in figure 2 when R is equal to 1 AU. Since the Earth's orbit around the Sun is not circular, Sun–Earth distance changes with time. In order to get the irradiance on a given day, a correction factor must be applied to the irradiance given for 1 AU. This correction factor ϵ is given by

$$\epsilon = (\overline{R}/r)^2 \tag{5}$$

where $\overline{R}$ is the value for 1 AU (1.496×10^8 km) et r is the Earth–Sun distance on a given day.

Using Kepler's laws, it is possible to compute the Sun–Earth distance on a given day (see for example Berger and Loutre, 1994) in order to obtain the correction factor (5). When these computations are done for every day of the year, the results can approximated by a trigonometric series (see Iqbal, 1983) such as

$$\begin{aligned} \epsilon &= 1.000110 + 0.034221 \cos\Gamma + 0.001280 \sin\Gamma \\ &\quad + 0.000719 \cos 2\Gamma + 0.000077 \sin 2\Gamma \end{aligned} \tag{6}$$

with

$$\Gamma = 2\pi(d_n - 1)/365 \tag{7}$$

The maximum error of this approximation is 1×10^{-4}. In equation (7) d_n is the day number starting at 1 on January 1 and ending at 365 on December 31, Γ being expressed in radians.

Figure 3 shows the eccentricity correction given by equation (6) as a function of the day number. It can be seen that an irradiance obtained at 1 AU can be modified by $\pm$ 3 % during a year. Such a geometrical variation is much more important than the observed fluctuations of the solar constant. When aeronomical computations are made for a specific day, it is always required to take this correction into account, since irradiance measurements are usually reduced to 1 AU. Furthermore, Figure 3 indicates that the Sun–Earth distance is the smallest around January 3 (highest irradiance) and the largest on July 4 (smallest irradiance).

4. DAILY MEAN IRRADIANCE

If we define the *solar zenith angle* χ also called *solar zenith distance* as the angle between the Earth–Sun direction and the local vertical at a given point, the irradiance received on a horizontal surface at that point is given by

$$E = E_s \times (\overline{R}/r)^2 \times \cos\chi \tag{8}$$

where E_s is the irradiance corresponding to a surface perpendicular to the incident radiation. The eccentricity correction given by equation (5) is include in equation(8).

The solar zenith angle can be expressed as a function of the *solar declination* δ, the latitude ϕ and the *solar hour angle* ψ by

$$\cos\chi = \sin\delta\sin\phi + \cos\delta\cos\phi\cos\psi \tag{9}$$

At sunrise, $\chi = 90°$. From equation (9) the hour angle at sunrise $\psi_\circ$ is than given by

$$\cos\psi_\circ = -\tan\phi \times \tan\delta \tag{10}$$

The daylight period is simply given by $2 \times \psi_\circ$.

The daily mean irradiance $\overline{E}$ can now be computed by integrating (8) between sunrise and sunset (see for example Kockarts, 2000)

$$\overline{E} = (E_s/\pi) \times (\overline{R}/r)^2 \times (\psi_0 \sin\phi\sin\delta + \sin\psi_0\cos\phi\cos\delta) \tag{11}$$

where E_s is the solar constant at 1 AU and the angle $\psi_\circ$ is defined by $\cos\psi_0 = -\tan\phi\tan\delta$. During polar nights, $\psi_0 = 0$ and during polar days of 24 hours $\psi_0 = \pi$.

For any application of equation (11) one has to know the declination δ which varies from +23.5° at Northern summer solstice to −23.5° at Northern winter solstice. For a period of 24 hours, the variation of the declination is always smaller the 0.5°. It is, therefore, acceptable to consider δ constant during a specific day. Exact values of the declination can be found in astronomical ephemerides. But there exist several excellent approximations. The following one leads to an error less than 3 arc seconds

$$\delta \quad = \quad (0.006918 - 0.399912\cos\Gamma + 0.070257\sin\Gamma$$

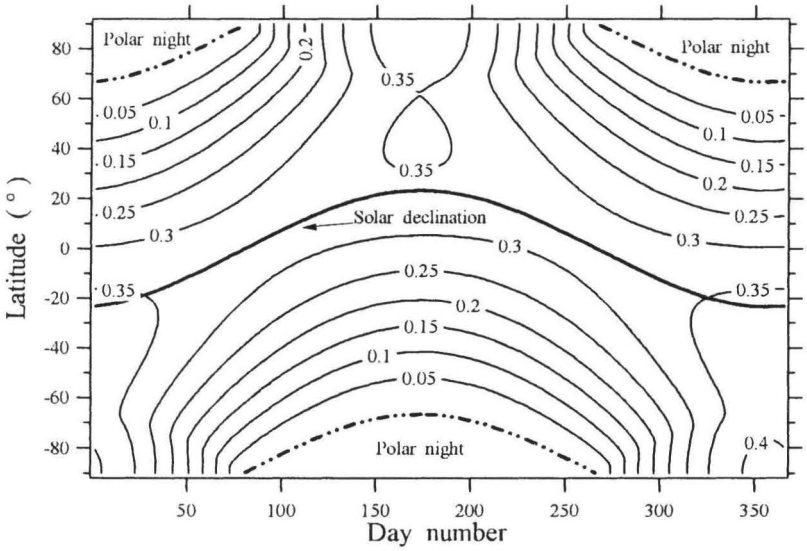

Figure 4. Isophotes of the daily mean irradiance, when E_s is arbitrarily taken equal to 1.

$$
\begin{aligned}
&- 0.006758 \cos 2\Gamma + 0.000907 \sin 2\Gamma \\
&- 0.002697 \cos 3\Gamma + 0.00148 \sin 3\Gamma)(180/\pi)
\end{aligned}
\tag{12}
$$

where Γ in radians is given by equation (7).

Equation (11) can now be used to compute isophotes of the daily mean irradiance shown on Figure 4. The solar constant E_s is arbitrarily taken equal to unity. In such a way, Figure 4 is valid for any wavelength of the solar spectrum. It is only necessary to multiply the numbers on the isophotes by the irradiance at that wavelength. Each isophote (full curves) gives the latitude at which a given irradiance is obtained as a function of the day number. It should be emphasized that these isophotes correspond to the top of the atmosphere where no absorption has taken place. The dashed curve gives the value of the solar declination δ computed with equation (12).

A careful examination of Figure 4 indicates the existence of an asymmetry between the two hemispheres. The Southern hemisphere receives more energy than the Northern one. This is a consequence of the Earth's orbital parameters. Satellite data analysis (Barlier *et al.*, 1974) have shown that many physical quantities present hemispherical asymmetries related to a larger amount of energy deposited in the Southern hemisphere.

5. SOLAR ACTIVITY

From Planck's law we know that a black body Sun emits at all wavelengths. However, at ground level only part of the spectrum can be observed (visible

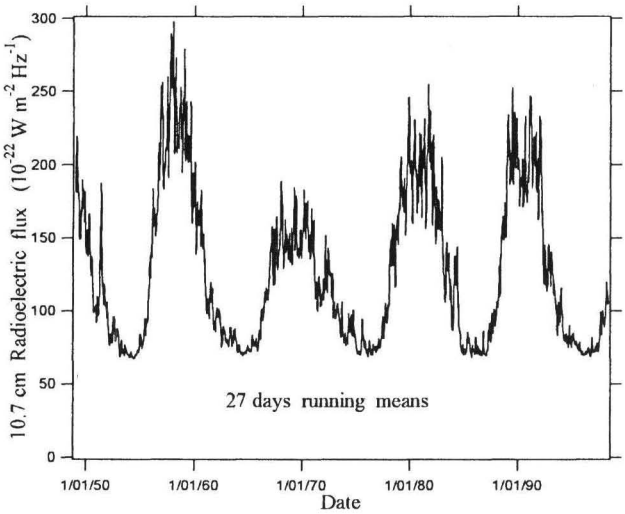

Figure 5. 10.7 cm Radio electric flux between 1949 an 1998.

and infrared). This is a consequence of the absorbing properties of molecular oxygen and ozone. The first spectrum above the ozone layer was obtained in 1946 with a spectrograph on board a V–2 rocket (Baum *et al.*, 1946). These measurements were extended in 1949 up to 112 km (Johnson *et al.*, 1952) essentially in order to measure, in the Harley bands around 280 nm, the vertical ozone distribution up to 70 km. These two historical papers stimulated further developments of the experimental techniques which were used on rockets and satellites.

After the invention of the telescope around 1610, Galileo observed dark spots on the Sun. During the 19th century observations of these sunspots lead to the conclusion that a periodicity of the order of 11 years exists in the solar activity. The Swiss astronomer Wolf introduced an index R called *Wolf number* or *Zürich sunspot number*. Since 1951, the sunspot number is derived at the Belgian Royal Observatory. Sunspot numbers are the longest time series available for a representation of solar activity.

Since 1948, an other index is measured in Canada, namely the 10.7 cm solar radio electric flux. Figure 5 shows the 27 day running means of this radio electric flux as a function of time. The data on figure 5 are 27 day running means because this period is the synodic period of rotation of the Sun. The 11 year periodicity is clearly apparent on this figure. However, it should be noted that two consecutive cycles have not necessarily the same amplitude. For example the maximum in 1958 is much larger than the maximum in 1969.

Although sunspot numbers and solar decimetric fluxes are extensively used in semi–empirical atmospheric models, they cannot provide a quantitative estimation of solar irradiance. Direct measurements are absolutely required. Using

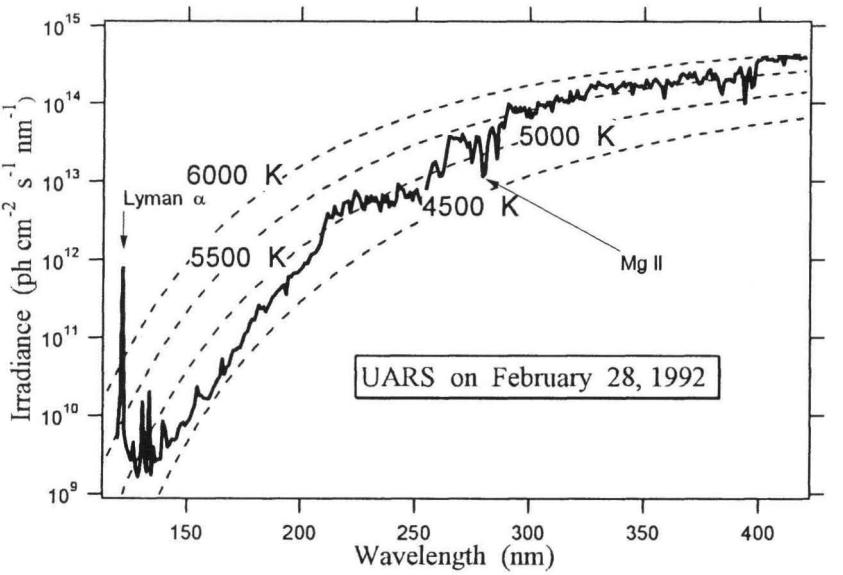

Figure 6. Solar irradiance as a function of wavelength.

these measurements, it is than possible to established relations between irradiance and indices.

As shown on Figure 2 the whole solar constant results from wavelength greater than 300 nm. Willson and Hudson (1991), using space–borne irradiance observations have shown that the total irradiance varies by about 0.1 % over the solar cycle. Such a variation is to be compared with the eccentricity effect discussed in section 3. Solar activity variations become more and more important as the wavelength decreases below 300 nm (Rottman, 1999).

As an example, Figure 6 for which numerical values were kindly provided by Gary Rottman (London *et al.*, 1993, Rottman, 1999) gives the irradiance measured by UARS (Upper Atmosphere Research Satellite) on February 28, 1992. Several features should be noted on this figure. Firstly, the irradiance is expressed in photons cm^{-2} s^{-1} nm^{-1}. This unit is simply obtained by dividing the energy unit of section 2 by the energy of the corresponding photon. Secondly, the dashed curves corresponding to various black body temperatures indicate that below 300 nm a single black body temperature cannot be used to compute irradiance. Thirdly, at 121.6 nm appears the intense Lyman-α line resulting from atomic hydrogen. Finally, the magnesium doublet line Mg II at 280 nm is indicated on the figure. This line is used to construct the Mg II index for modeling solar activity effects on irradiance. Other indices based on He I line at 1083 nm or on Ca II K line at 393 nm. The solar cycle variation of the irradiance shown on Figure 6 is discussed by Rottman (1999). The solar Lyman–α line increases from 3.0×10^{11} ph cm^{-2} s^{-1} at solar minimum to 6.7×10^{11} ph cm^{-2} s^{-1} at solar maximum (Tobiska *et al.*, 1997, Woods and Rottman, 1997) i.e. a variation of a factor of two.

Lean (1991) concludes that for X rays and wavelengths $\lambda < 10$ nm, irradiance variation during a solar cycle can change by a factor 10 to 1000. In the range 10 to 120 nm the irradiance can increase by a factor 2 to 10 between solar minimum and solar maximum. Between 125 and 175 nm the increase is of the order of 50 % . In the Schumann–Runge bands (175 to 205 nm) of molecular oxygen, the variation can be of the order of 15 % whereas between 205 and 250 nm it is of the order of 4 % .

Below 100 nm the situation becomes more complex. The solar spectrum is characterized by numerous emission lines and there are serious discrepancies between existing measurements. Furthermore, the variations with solar activity increase. Richards *et al.* (1994) have, however, developed an extreme ultraviolet (EUV) model based on existing measurements and using the 10.7 cm index. This model is suitable for aeronomical calculations.

6. PRIMARY ACTIONS OF SOLAR RADIATION

When a photon with energy $h\nu$, h being Planck's constant and ν being the frequency of the radiation, penetrates into the atmosphere three primary actions are possible depending on the energy and on the nature of the atmospheric constituents:

1. Excitation followed by *resonant emission* at the same wavelength or by *fluorescent emission* at a longer wavelength. This mechanism can occur for an atom X as well as for a molecule X_2 or XY

$$\begin{array}{lcl} X + h\nu & \rightarrow & X^* \rightarrow X + h\nu \quad \text{(resonance)} \\ & \text{or} & \\ X + h\nu & \rightarrow & X^* \rightarrow X^\dagger + h\nu_1 \quad (\nu_1 < \nu \ \text{ fluorescence}) \end{array} \tag{13}$$

   In these processes X^* et $X^\dagger$ are excited atoms. A well known example is Lyman–α geocoronal emission resulting from absorption of the solar Lyman–α line at 121.6 nm by atmospheric atomic hydrogen which reemits this line resonantly.

2. Photodissociation of a molecule XY or X_2

$$\begin{array}{lcl} XY + h\nu & \rightarrow & X + Y \\ XY + h\nu & \rightarrow & X^* + Y \\ XY + h\nu & \rightarrow & X^* + Y^* \end{array} \tag{14}$$

   where X^* and Y^* are excited states.

   For example, O_2 can be photodissociated for wavelengths shorter than 242.4 nm leading to two oxygen atoms in their ground state $O(^3P)$. However, if the wavelength is shorter than 175 nm, one atom is in its ground state but the other is in an excited state $O(^1D)$. This excited state can emit the airglow red line at 630 nm.

3. Photoionization of an atom or a molecule

$$\begin{array}{ccc} X + h\nu & \rightarrow & X^{+} + e \\ & \text{ou} & \\ X + h\nu & \rightarrow & X^{\dagger +} + e \end{array} \tag{15}$$

X^{+} is a positive ion in its ground state, $X^{\dagger +}$ is an excited ion and e is an electron.

For example, O_2 is photoionized for $\lambda < 102.7$ nm, H for $\lambda < 91.1$ nm, O for $\lambda < 91$ nm, N_2 for $\lambda < 79.6$ nm and He for $\lambda < 50.4$ nm. As a consequence, all atmospheric constituents which are or become major constituents at some height in the atmosphere are only ionizable for wavelength shorter than 100 nm. Minor constituents do not contribute to the direct ionization of the atmosphere. Nitric oxide (NO) is the sole exception since it can be ionized by Lyman–α which penetrates into the mesosphere.

These primary actions require a knowledge of the capacity that an atmospheric constituent has to absorb radiation. This means that we have to know the absorption and ionization cross sections usually expressed in cm^2.

Figure 7 (upper panel) shows the absorption cross sections for O_2 and O_3 averaged over 500 cm^{-1} wavenumber intervals. The small O_2 cross section at Lyman–α indicates that this radiation can penetrate deep into the atmosphere. The dashed curve delimited by the two symbols SR corresponds to the Schumann–Runge band system of molecular oxygen. Average values cannot be adopted in this region as will be discussed in section 8. Molecular nitrogen does not appear on this figure, since that major atmospheric component does not absorb above 100 nm. Absorption cross sections for numerous minor constituents are regularly compiled by DeMore *et al.* (1997).

The absorption cross sections used in the EUV model of Richards *et al.* (1994) are given on Figure 7 (lower panel) for O, O_2 and N_2. The symbols correspond to specific solar lines and the cityscape curves give an average cross section for 5 nm intervals. It is useful to note the different vertical scales on the two panels. Absorption cross sections are usually higher in the EUV than in the UV range.

7. OPTICAL DEPTH

In order to study the effects of solar radiation on the atmosphere, one has to know how and where a specific radiation is absorbed. When an atmospheric constituent, with concentration n_j, is capable to absorb a photon flux $\Phi(\lambda)$ at wavelength λ, the decrease of the flux over an elementary distance ds is given by

$$d\Phi(\lambda) = -n_j \times \Phi(\lambda) \times \sigma_{a,j}(\lambda)\, ds \tag{16}$$

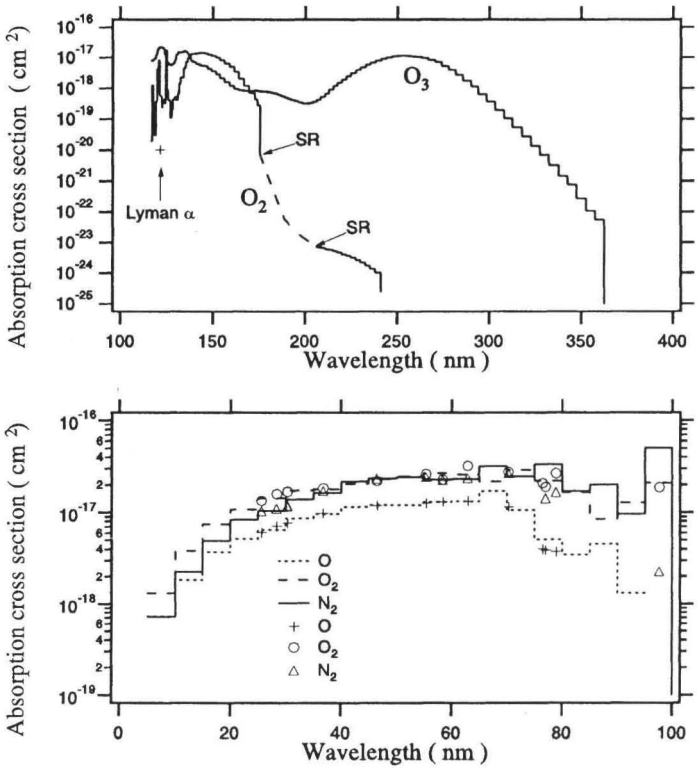

Figure 7. Absorption cross sections for wavelengths $\lambda > 100$ nm (upper panel) and $\lambda < 100$ nm (lower panel).

where $\sigma_{a,j}(\lambda)$ is the absorption cross section at wavelength λ. Integration of (16) between altitude z and infinity, along the optical path s, leads to

$$\Phi(\lambda) = \Phi_\infty(\lambda) \times \exp[-\int_z^\infty \sigma_{a,j}(\lambda) \times n_j(s)]\, \mathrm{d}s \tag{17}$$

where $\Phi_\infty(\lambda)$ is the photon flux (number of photons $\mathrm{cm}^{-2}\ \mathrm{s}^{-1}$) available at the top of the atmosphere.

Equation (17) is Beer–Lambert's law which is strictly valid for a single wavelength. However, in aeronomy equation (17) is applied for wavelengths intervals $\Delta\lambda$, since solar fluxes are usually known with a lesser resolution than absorption cross sections.

The *optical depth* $\tau_j(\lambda)$, for a constituent j along the line of sight s, is defined by

$$\tau_j(\lambda) = \int_z^\infty \sigma_{a,j}(\lambda) \times n_j(s)\ \mathrm{d}s = \sec\chi \int_z^\infty \sigma_{a,j} \times n_j(z)\ \mathrm{d}z \tag{18}$$

where χ is the solar distance and $\mathrm{d}s = \mathrm{d}z/\cos\chi$, $\mathrm{d}z$ being the elementary length

along the vertical. The cross section $\sigma_{a,j}$ is under the integral sign in equation (18), since it can depend on temperature and so, it is altitude dependent.

When several absorbing species, at wavelength λ, are present, the total optical depth $\tau(\lambda) = \sum_j \tau_j(\lambda)$ is obtained by summing equation (18) over the various constituents j.

If the photon energy is sufficient to photodissociate a molecule j, the *photodissociation coefficient* $J_j(\mathrm{s}^{-1})$ is given by

$$\begin{aligned} J_j(\lambda) &= \sigma_{a,j}(\lambda) \times \Phi_\infty(\lambda) \exp -[\tau(\lambda)] \\ &= J_{\infty,j}(\lambda) \exp -[\tau(\lambda)] \end{aligned} \tag{19}$$

where $J_{\infty,j}(\lambda)$, expressed in s^{-1}, is the photodissociation coefficient at the top of the atmosphere. Since other constituents than species j can absorb, the optical depth in equation (19) must be the total optical depth.

The total photodissociation coefficient $J_{tot}(z)$ at a given height z is

$$J_{tot,j}(z) = \int_0^\infty J_j(\lambda, z)\, \mathrm{d}\lambda \tag{20}$$

Similarly, the *photoionization coefficient* I is defined by

$$\begin{aligned} I_j(\lambda) &= \sigma_{i,j}(\lambda) \times \Phi_\infty(\lambda) \exp -[\tau(\lambda)] \\ &= I_{\infty,j}(\lambda) \exp -[\tau(\lambda)] \end{aligned} \tag{21}$$

where $\sigma_{i,j}(\lambda)$ is the ionization cross section for constituent j and $I_{\infty,j}(\lambda)$ en s^{-1} is the ionization coefficient at the top of the atmosphere. The total ionization coefficient is obtained by a relation similar to (20).

For a given wavelength, the relation $\sigma_{i,j}(\lambda) \leq \sigma_{a,j}(\lambda)$ is always true. In equation (21), the optical depth must always be computed with absorption cross sections. Expressions (20) and (21) are valid if the *quantum yield* of a specific process is one. Although some dissociation processes are energetically possible, laboratory measurements show that a smooth transition occurs between the dissociation limit and some shorter wavelength. In that region, the quantum yield increases from 0 to 1. A good example is given in the photodissociation of O_3 which for $\lambda < 411$ nm could lead to the production of excited atomic oxygen $O(^1D)$. Laboratory measurements (see DeMore *et al.*, 1997) show that a vary small quantum yield exists around 340 nm and increases to practically 1 around 300 nm. Furthermore, this quantum yield is temperature dependent.

For a given species j, photodissociation or photoionization leads to a loss rate L_j in $\mathrm{cm}^{-3}\ \mathrm{s}^{-1}$ given by

$$\begin{aligned} L_j &= n_j \times J_j \\ &\text{ou} \\ L_j &= n_j \times I_j \end{aligned} \tag{22}$$

where n_j in cm^{-3} is the concentration of the initial species.

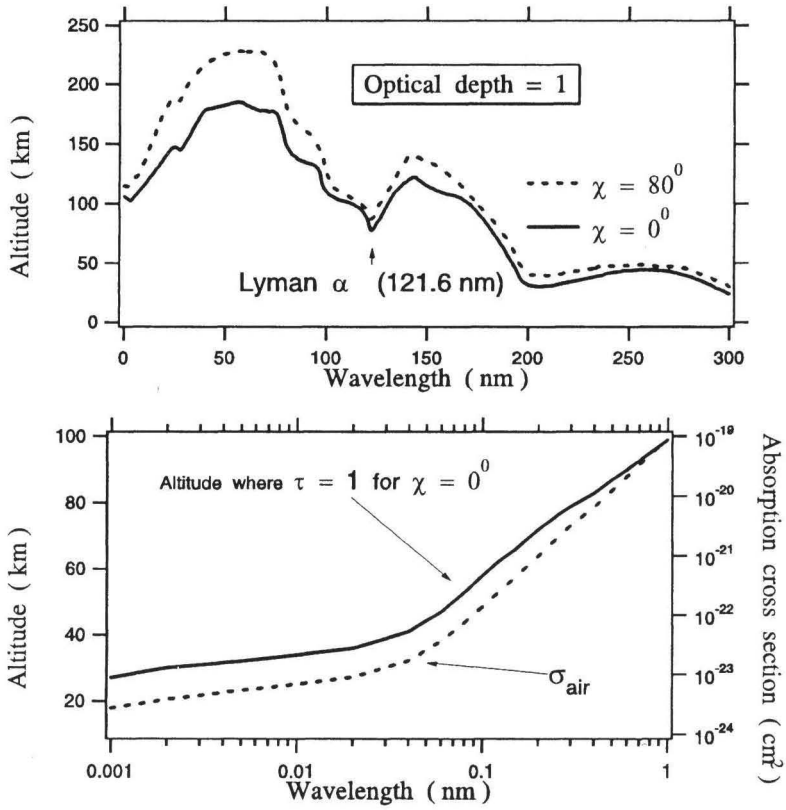

Figure 8. Altitude where $\tau = 1$ for wavelengths $\lambda > 1$ nm (upper panel) and $\lambda < 1$ nm (lower panel).

In the case of photodissociation of a homonuclear diatomic molecule, like O_2, the production rate P of atoms is twice the loss rate of molecules

$$P(\mathrm{O}) = 2 \times L(\mathrm{O}_2) = 2 \times n(\mathrm{O}_2) \times J(\mathrm{O}_2) \tag{23}$$

It is possible to show that production rates and loss rates reach a maximum at the altitude where the corresponding optical depth is 1.

Figure 8 (upper and lower panel) shows the altitude where $\tau = 1$ as a function of wavelength. Several important features can be seen on this figure. On the upper panel one notices that the major effect of solar radiation between 200 and 300 nm occurs in the stratosphere below 50 km altitude. This radiation does not reach ground level because of O_3 absorption (see Figure 7).Between 100 and 200 nm solar radiation is essentially absorbed in the mesosphere and lower thermosphere. The figure clearly shows that Lyman–α at 121.6 nm can deeply penetrate in the mesosphere. This radiation plays a fundamental role in the formation of the ionospheric D–layer where it can ionize nitric monoxide NO. Below 100 nm solar energy is deposited in the thermosphere where it is

responsible for the formation of the ionosphere. This results from the fact that the ionization potentials for all major constituents correspond to wavelengths < 100 nm. Furthermore, the sharp temperature gradients observed in the lower thermosphere are a consequence of the absorption of EUV radiation by neutral constituents. The dashed curve in the upper panel corresponds to a solar zenith angle of 80°. Since optical depth increases with solar zenith distance, it is logical that unit value is reached at a higher altitude.

The lower panel of Figure 8 gives the altitude where unit optical depth is encountered for solar X–rays which can penetrate down to the stratosphere. This is a consequence of the low absorption cross of O_2 and N_2 below 1 nm. The right hand scale gives the air cross section $\sigma_{\text{air}} = 0.78 \times \sigma_{N_2} + 0.21 \times \sigma_{O_2} + 0.01 \times \sigma_{\text{Ar}}$.

A final remark should be made for the use of $\sec\chi$ in the expression of the optical depth. When the Sun is on the horizon $\sec 90° = \infty$. Actually the use of $\sec\chi$ implies that the Earth is considered as flat! Chapman (1931) solved this problem by introducing a function (now called Chapman function) for large zenith angles. This function is not analytically integrable. Various approximations have been developed (see for example Smith III and Smith, 1972). However, the original derivation by Chapman implies that the absorbing constituent decreases exponentially with a scale height. Therefore, application of Chapman's function to ozone absorption in the stratosphere can lead to errors since this constituent does not uniformly decrease exponentially.

8. A FEW PROBLEMS WITH THE CROSS SECTIONS

All molecules are characterized by a spectral signature composed of electronic, vibrational and rotational lines. If an absorption spectrum in a certain wavelength region shows the presence of numerous lines, it can be unsafe to use averaged values for the absorption cross sections. Molecular oxygen provides a good example of such a situation.

Figure 9 shows a schematic view of some potential energy curves of O_2 as a function of the internuclear distance of the two oxygen atoms. On the right hand side, the first two limits of dissociation (242.4 and 175 nm) of O_2 are indicated as well as the states of the resulting atoms. The Schumann–Runge absorption band system corresponds to the transitions between the ground state $X^3\Sigma_g^-$ and the excited state $B^3\Sigma_u^-$ in the wavelength region 175–205 nm. The dashed curves correspond to repulsive states which can lead to predissociation. Using high resolution absorption measurements, Minschwaner *et al.* (1992) have deduced a set of polynomial coefficients which can be used to compute the absorption cross sections with a resolution of 0.5 cm^{-1} for temperatures ranging from 130K to 500K.

As an example, Figure 10 gives the O_2 absorption cross section in the Schumann-Runge bands for 300 K. The band structure is clearly seen and the cross section can change by several orders of magnitude over very short wavelength intervals. The results of Figure 10 have been computed every 0.5 cm^{-1} and the figure contains, therefore, 16000 points. Such a computation

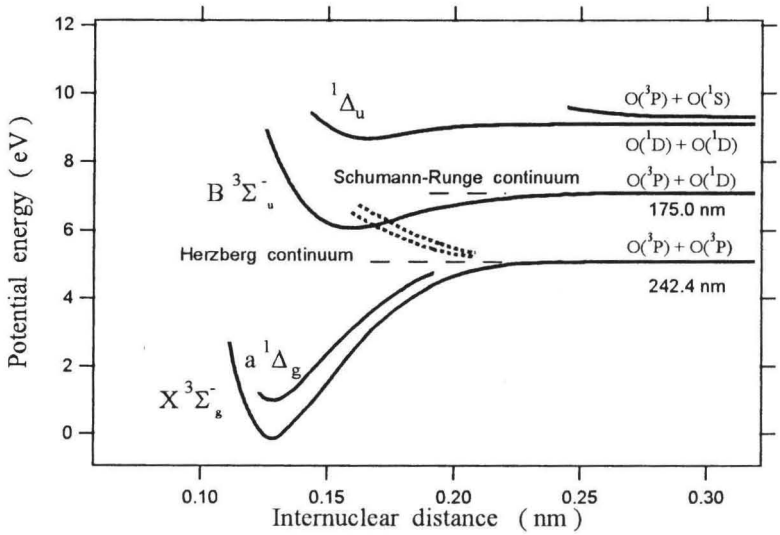

Figure 9. Potential energy curves of O_2.

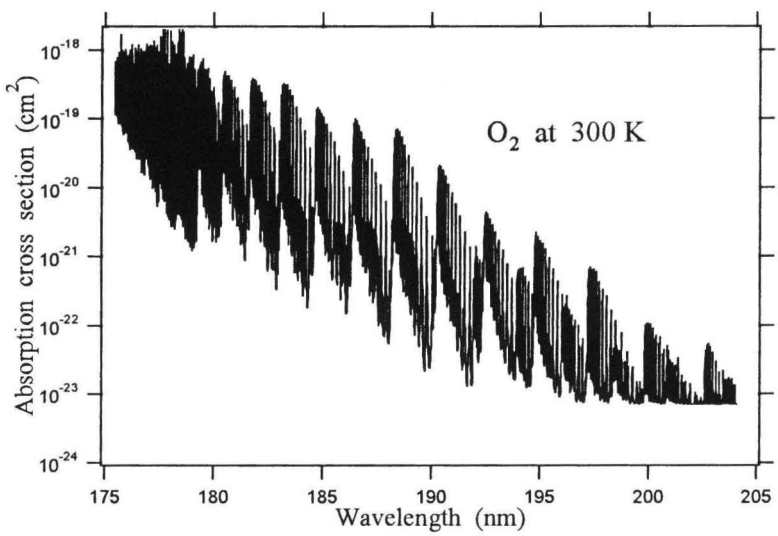

Figure 10. Molecular oxygen absorption cross section In the Schumann--Runge bands for 300 K.

can be made for any altitude or any temperature in the homosphere. But if these results have to used to compute the penetration of solar radiation in an atmospheric model, the computational cost can become extremely high.

Recently, Kockarts (1994) has developed a robust approximation to compute photodissociation coefficients for O_2 and any other minor coefficient except NO for which the reader should use the parameterization of Minschwaner and Siskind (1993).

We will briefly sketch how this robust approximation can be obtained. The spectral interval of the Schumann-Runge bands (49 000 cm^{-1} to 57 000 cm^{-1}) is divided in 16 subintervals of 500 cm^{-1}. Wavenumber unit has been adopted since energy varies linearly with wavenumber. This is not the case for wavelengths. With the definition of the solar flux available at a given height (equation 17) and expression (19) for the photodissociation coefficient, it is possible to define two *reduction factors* in every 500 cm^{-1} wavenumber interval such as

$$R_i(\mathrm{M}) = \frac{1}{1000} \sum_{j=1}^{1000} \exp\left(-\tau_{ji}\right) \tag{24}$$

and

$$R_i(\mathrm{O_2}) = \frac{1}{1000} \sum_{j=1}^{1000} \sigma_{ji} \exp\left(-\tau_{ji}\right) \tag{25}$$

where τ_{ji} is given by

$$\tau_{ji} = \int_s^{\infty} \sigma_{ji} n(\mathrm{O_2})\, \mathrm{d}s \tag{26}$$

In each interval i, 1000 cross sections of O_2 are used i.e 16 000 values for the complete Schuman–Runge system.

The solar flux $\phi_i(z)$ available at a given altitude z and in an interval i is now given by

$$\phi_i(z) = \phi_i(\infty) \times R_i(\mathrm{M}) \times \exp\left[-\tau_i(\mathrm{O_3})\right] \tag{27}$$

where $\phi_i(\infty)$ is the slant optical depth due to ozone absorption in the same interval.

The photodissociation coefficient $J_i(\mathrm{M})$ for any minor constituent M is computed from

$$J_i(\mathrm{M}) = \phi_i(z) \times \sigma_i(\mathrm{M}) \tag{28}$$

where $\sigma_i(\mathrm{M})$ is the absorption cross section for M in interval i.

The photodissociation coefficient for O_2 is the obtained from

$$J_i(\mathrm{O_2}) = \phi_i(\infty) \times R_i(\mathrm{O_2}) \times \exp\left[-\tau_i(\mathrm{O_3})\right] \tag{29}$$

Computations of the reduction factor are time consuming in this procedure. The reduction factors are a sum of 1000 exponentials with negative arguments. Therefore, Kockarts (1994) made a non linear least square fit to the exact computations under the form

$$R_i(\mathrm{M}) = a_1 \times \exp\left(-a_2 \times N\right) + \ldots a_{11} \times \exp\left(-a_{12} \times N\right) \tag{30}$$

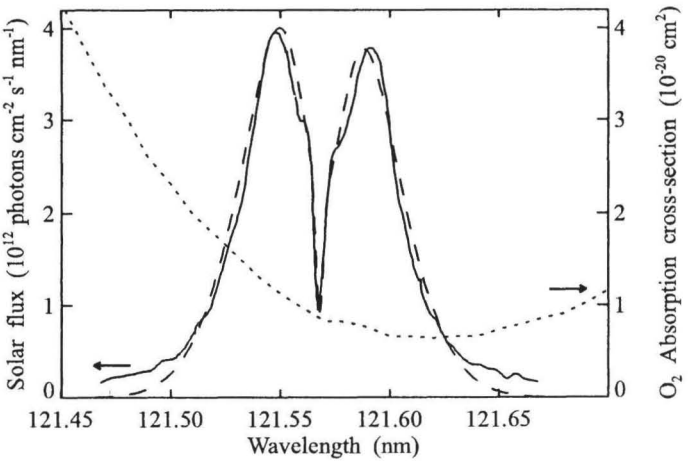

Figure 11. Lyman--α line profile and O_2 absorption cross section.

where N is the slant O_2 total content. An identical expression with coefficients b_1 to b_{12} was used for $R_i(O_2$. The coefficients resulting from the fit can be found in Kockarts(1994). Instead of computing 1000 exponentials in each interval, the approximation requires only to compute 6 exponentials. The accuracy over the whole Schumann–Runge system is of the order of $\pm 2\%$. The approximation is robust since all terms are decreasing exponentials when the total content of O_2 increases.

As stated earlier, the approximation developed by Minschwaner and Siskind (1993) must be used for NO since the absorption spectrum of this minor constituent has so many lines in the Schumann–Runge wavelength region that on cannot use average cross sections in equation (28).

Another situation occurs when the cross section varies smoothly but the solar flux changes rapidly over a short wavelength interval. This case has been analyzed by Chabrillat and Kockarts (1997,1998) for the solar Lyman–α line. The full line on Figure 11 shows a profile of Lyman–α measured by Lemaire *et al.* (1978) for quiet Sun conditions. The decrease in intensity at the center of the line results from absorption by geocoronal hydrogen. Chabrillat and Kockarts (1997) fitted this line by a sum of three gaussian functions. The result is given by the dashed line. On the same figure the absorption cross section of O_2 (Lewis *et al.*, 1983) is plotted as a function of wavelength (right hand axis). This cross section is also temperature dependent.

In most aeronomical applications, the cross section of molecular oxygen is taken as constant with a value of 10^{-20} cm^2 and a value of 3×10^{11} photons cm^{-2} s^{-1} is adopted for the total solar Lyman–α irradiance. Using the technique of the reduction factors, Chabrillat and Kockarts (1997) showed that with a sum of three exponentials an exact calculation with the data of Figure 11 can be approximated with error smaller than 0.5% for R(M) and less than 2% for

$R(O_2)$. This last two reduction factors have the same meaning than those defined for the Schumann–Runge bands.

Use of a constant cross section for molecular oxygen can lead to an underestimation as large as 20% for the total photodissociation coefficient of water vapor around 65 km and to an underestimation between 20% and 100% for the total photodissociation of methane below 70 km altitude. Photodissociation of CO_2 and photoionization of NO are also strongly affected.

9. CONCLUSION

Although we learned a lot on the aeronomical effects of solar radiation, this tutorial paper has tried to show that still many improvements are required to understand the whole phenomena related to solar radiation. In a broad sense they can schematized as follow:

1. More measurements of UV and EUV solar radiation are required. The EUV part of the spectrum below 100 nm is particularly important.

2. Although the total irradiance of the Lyman–α over a solar cycle is rather well known, the evolution of the detailed profile with solar activity is poorly known.

3. The temperature dependence of the absorption cross sections is not always sufficiently known and higher wavelength resolution is required.

Let's hope that there will still be young scientists interested in those type of questions.

REFERENCES

Barlier F., Bauer P., Jaeck C., Thuillier G. and Kockarts G., *J. Geophys. Res.* **79** (1974) 5273–5285.

Baum W.A., Johnson F.S., Oberly J.J., Rockwood C.C., Strain C.V. and Tousey R., *Phys. Rev.* **70** (1946) 781–782.

Berger A. and Loutre M.F., Long–term variations of the astronomical seasons. In: *ERCA Volume 1, Topics in Atmospheric and Interstellar Physics and Chemistry*, edited by C. Boutron (EDPD Sciences, Les Ulis France, 1994) pp.33–61.

Bose S., *Z. für Physik* (1924) translated in *American Journal of Physics* **44** (1976) and reproduced in *J. Astrophys. Astr.* **15** (1994) 3–11.

Chabrillat S. and Kockarts G., *Geophys. Res. Lett.* **24** (1997) 2659–2662 and printing error **25** (1998) 79.

Chapman S., *Proc. Phys. Soc.* **43** (1931) 483–501.

Chapman S. and Milne E.A., *Quart. J. Roy. Meteorol. Soc.* **46** (1920) 357–398.

DeMore W.B., Sander S.P., Golden D.M., Hampson R.F., Kurylo M.J., Howard C.J., Ravishankara A.R., Kolb C.E. and Molina M.J. *JPL Publication* **97-4** (1997) 1–269.

Iqbal M., *An introduction to solar radiation* (Academic Press, 1983)

Johnson F.S., Purcell J.D., Tousey, R. and Watanabe K., *J. Geophys. Res.* **57** (1952) 157–176.

Kockarts G., *Space Sci. Reviews* **14** (1973) 723–757.

Kockarts G., *Ann. Geophysicae* **12** (1994) 1207–1217.

Kockarts G., *Aéronomie: Physique et chimie de l'atmosphère* (DeBoeck Université, Bruxelles, 2000)

Lean J., *Rev. Geophys.* **29** (1991) 505–535.

Lemaire P., Charra J., Jouchoux A., Vidal–Madjar A., Artzner G.E., Vial J., Bonnet R.M. and Skumanich A., *Astrophys. J.* **223** (1978) L55–L58.

Lewis B.R., Varvadas I.M. and Carver J.H., *J. Geophys. Res.* **88** (1983) 4935–4940.

Lilensten J., The Polar Lights in the Solar System. In: *ERCA Volume 2, Physics and Chemistry of the Atmospheres of the Earth and Other Objects of the Solar System*, edited by C. Boutron (EDPD Sciences, Les Ulis France, 1996) pp.329–344.

Lilensten J. et Blelly P.–L., *Du Soleil à la Terre: Aéronomie et météorologie de l'espace* (Presses Universitaires de Grenoble, 1999)

London J., Rottman G., Woods T.N. and Wu F., *Geophys. Res. Lett.* **20** (1993) 1315–1318.

Minschwaner K., Anderson G.P., Hall L.A. and Yoshino K., *J. Geophys. Res.* **97** (1992) 10 103–10 108.

Minschwaner K. and Siskind D.E., *J. Geophys. Res.* **98** (1993) 20 401–20 412.

Planck M., *Annalen der Physik, Vierte Folge*, **4** (1901) 553–563.

Richards P.G., Fennelly J.A. and Torr D.G., *J. Geophys. Res.* **99** (1994) 8981–8992.

Rottman G., *J. Atmos. Solar–Terr. Phys.* **61** (1999) 37–44.

Smith III F.L. and Smith C., *J. Geophys. Res.* **77** (1972) 2592–2597.

Tobiska W.K., Pryor W.R. and Ajello J.M., *Geophys. Res. Lett.* **24** (1997) 1123–1126.

Willson R.C. and Hudson, H.S., *Nature* **351** (1991) 42–44.

Woods T.N. and G.J. Rottman, *J. Geophys. Res.* **102** (1997) 8769–8779.